Contents lists available at ScienceDirect

### **Computer Physics Communications**

journal homepage: www.elsevier.com/locate/cpc



## Arbitrarily high-order unconditionally energy stable SAV schemes for gradient flow models



Yuezheng Gong <sup>a</sup>, Jia Zhao <sup>b,\*</sup>, Qi Wang <sup>c</sup>

- <sup>a</sup> College of Science, Nanjing University of Aeronautics and Astronautics, Nanjing 210016, China
- <sup>b</sup> Department of Mathematics & Statistics, Utah State University, Logan, UT, 84322, USA
- <sup>c</sup> Department of Mathematics, University of South Carolina, Columbia, SC, 29208, USA

#### ARTICLE INFO

# Article history: Received 21 July 2019 Received in revised form 31 October 2019 Accepted 4 November 2019 Available online 11 November 2019

Keywords: Unconditional energy stability Scalar auxiliary variable High order schemes Gradient flow models

#### ABSTRACT

We propose a family of novel, high-order numerical schemes for gradient flow models based on the scalar auxiliary variable (SAV) approach and name them the high-order scalar auxiliary variable (HSAV) methods. The proposed schemes are shown to reach arbitrarily high order in time while preserving the energy dissipation rate and thereby being unconditionally energy stable. When the HSAV strategy is applied to thermodynamically consistent gradient flow models, we arrive at semi-discrete high-order, unconditionally energy-stable schemes. We then employ the Fourier pseudospectral method in space to arrive at fully discrete unconditionally energy stable schemes. A few selected HSAV schemes are tested against three benchmark problems to demonstrate the accuracy, efficiency and unconditional energy stability of the schemes. The numerical results confirm the expected order of accuracy and robustness in much larger time steps than the low order SAV schemes.

© 2019 Elsevier B.V. All rights reserved.

#### 1. Introduction

Dynamics of a dissipative system is determined by a free energy, a set of conservation laws, and the mobility leading to energy decay in time [1–4]. In the literature, when the conservation laws are absent, models describing dissipative dynamics are often called gradient flow models. In general, we consider thermodynamic variable  $\phi(\mathbf{x},t)$  for a dissipative system in domain  $\mathbf{x}\in\Omega$ . The evolution (dynamic) equation for  $\phi(\mathbf{x},t)$  can be formulated based on the Onsager linear response theory as follows [5]

$$\partial_t \phi(\mathbf{x}, t) = \mathcal{G} \frac{\delta F}{\delta \phi},\tag{1}$$

where  $\mathcal G$  is the mobility, a negative semi-definite differential or integral operator which may depend on  $\phi$ . Here F is the free energy, and  $\frac{\delta F}{\delta \phi}$  is the variational derivative of F with respect to  $\phi$ , called the chemical potential. For instance, if  $F=F[\phi,\nabla\phi]$ , the chemical potential is given by  $\frac{\delta F}{\delta \phi}=\frac{\partial F}{\partial \phi}-\nabla\cdot\left(\frac{\partial F}{\partial \nabla\phi}\right)$ . In this paper, we present our results using periodic boundary conditions for simplicity. System (1) is a general gradient flow model, which admits an intrinsic energy dissipation law

$$\frac{dF}{dt} = \int_{\Omega} \left(\frac{\delta F}{\delta \phi}\right)^{\mathsf{T}} \mathcal{G} \frac{\delta F}{\delta \phi} d\mathbf{x} \le 0, \tag{2}$$

due to the negative semi-definite property of G.

E-mail addresses: gongyuezheng@nuaa.edu.cn (Y. Gong), jia.zhao@usu.edu (J. Zhao), qwang@math.sc.edu (Q. Wang).

Note that the gradient flow model is specified by the triple  $(\phi,\mathcal{G},F)$ . Many dissipative PDE models are special cases of general gradient flow model (1). For instance, if we specify the mobility as  $\mathcal{G}=-M$  (with M a positive constant) and a double well free energy  $F=\int_{\Omega}\left[\frac{1}{2}|\nabla\phi|^2+\frac{1}{4\varepsilon^2}(\phi^2-1)^2\right]d\mathbf{x}$  (with  $\varepsilon$  a free parameter), the general gradient flow model (1) reduces to the well-known Allen–Cahn equation with the double well potential [6]

$$\partial_t \phi = -M \left( -\Delta \phi + \frac{1}{c^2} (\phi^3 - \phi) \right). \tag{3}$$

If we specify the mobility as  $G = M\Delta$ , we end up with the well-known Cahn-Hilliard equation [7]

$$\partial_t \phi = M \Delta \left( -\Delta \phi + \frac{1}{\varepsilon^2} (\phi^3 - \phi) \right). \tag{4}$$

There are many more examples such as the molecular beam epitaxy (MBE) growth models [8,9], phase field crystal models [10], dendritic crystal growth models [11], multiphase models [12,13], etc. For a detailed discussion, readers can refer to [3] and the references therein.

For gradient flow models, many accurate, efficient and stable numerical schemes have been developed, among which the ones that preserve the energy dissipation property at the discrete level, known as energy stable schemes, are especially appealing. If such a numerical stability does not have any restrictions on the time step, it is called unconditionally energy stable. For this class of numerical schemes, a large body of works have been done recently, for example the energy stable algorithms presented in

<sup>\*</sup> Corresponding author.

the following papers [8.14–28] and the references therein. However, many of these schemes are problem-specific, depending on the specific structures/properties of  $\mathcal{G}$  and F. Recently, inspired by [27,28], Yang et al. [3,29-32] proposed an energy quadratization (EQ) approach for dealing with general gradient flow models to obtain linear energy stable schemes. Shen et al. [5,33] then further extended the EO idea to develop the scalar auxiliary variable (SAV) approach, where the resulting linear schemes can be solved quickly by the fast Fourier transform (FFT). The basic idea of both EQ and SAV is to introduce some auxiliary variables to reformulate a gradient flow model into an equivalent form, where the reformulated free energy is a quadratic functional. Then linear and unconditionally energy stable schemes can be developed in a generic fashion for the reformulated system, which in turn approximates the original gradient flow model. Due to the generality of the EQ and SAV approaches, they have been applied for many existing gradient flow models recently [5,9,25,26,29,34].

However, most of the existing energy stable schemes are up to second-order accuracy in time. There is little work on developing higher order energy stable schemes. Since gradient flow models sometimes require longtime dynamical simulations to reach steady states, high-order accurate, efficient, energy stable schemes sustaining long time simulations are always desirable. Several seminal works on developing high-order energy-stable numerical schemes have been reported lately [35-37]. In this paper, we combine the SAV idea with the Runge-Kutta (RK) methodology to develop arbitrarily high-order energy-stable numerical schemes for general gradient flow models. Firstly, we use the SAV technique to transform the gradient flow model into an equivalent form with a quadratic free energy functional along with an equivalent energy dissipation law. Secondly, we exploit the structure-preserving Gaussian collocation method and corresponding RK method to derive high-order scalar auxiliary variable (HSAV) schemes, which are proven rigorously to preserve a discrete energy dissipation law. Note that the newly proposed high-order schemes overcome all the shortcomings of the convex-splitting RK scheme in [35]. For instance, by using the SAV technique, our approach does not have any restrictions on specific forms of mobility G and free energy F, making it applicable to any gradient flow models. Moreover, by employing the Gaussian collocation method, our approach can reach arbitrarily high-order accuracy in time with optimal RK stages.

Energy stable schemes in general are defined as the numerical schemes that warrant energy decay in discrete time without mentioning the details on how this decay is achieved. Some energy quadratization methods (EQ(IEQ) and SAV altogether) in fact respect the discrete energy dissipation rate with respect to the discrete energy definition within the range of the truncation error. It therefore captures the transient dynamics more accurately by accounting for the detailed energy budget. This issue has not been discussed before for any other types of energy stable schemes. Most of the non-EQ based energy stable schemes achieve energy stability by modifying the energy dissipation rate or the discrete energy. That can alter the transient dynamics within the range of truncation error. For long time numerical simulation, it could inevitably introduce a large numerical error if the error propagation is not well-controlled. In this regard, the EQ-based energy stable schemes demonstrate a competitive edge.

The rest of this paper is organized as follows. In Section 2, we will present the general gradient flow model and its EQ reformulation based on the SAV approach. In Section 3, we derive the high-order time discretization for the reformulated system and prove its unconditional energy stability. In Section 4, we use the Fourier pseudo-spectral method for the spatial discretization to arrive at fully discrete schemes, which are unconditionally energy stable as well. Several numerical examples are presented in Section 5. In the end, we give the concluding remarks.

#### 2. Gradient flow models and their SAV reformulation

In this section, we begin with a general gradient flow model and apply the energy quadratization approach to arrive at an equivalent form with a quadratic energy functional and the energy dissipation law. We implement the process using the SAV method and name the reformulated system the SAV reformulation. The SAV reformulation for the gradient flow models provides an elegant platform for developing arbitrarily high-order unconditionally energy stable schemes, which is the major focus of this paper.

#### 2.1. General gradient flow models

Consider the domain  $\Omega$  with enough regularity on the boundary. The  $L^2$  inner product and its norm are defined as  $\forall f,g\in L^2(\Omega)$ ,  $(f,g)=\int_{\Omega}fgd\mathbf{x}$  and  $\|f\|_2=\sqrt{(f,f)}$ , respectively. For simplicity, we illustrate the idea using a single state variable  $\phi$ . Dynamics of  $\phi$  is governed by a free energy or Lyapunov function F and a negative semi-definite mobility operator  $\mathcal{G}$ :

$$\partial_t \phi = \mathcal{G} \frac{\delta F}{\delta \phi}.\tag{5}$$

The generic form of the free energy F is written as

$$F = \frac{1}{2}(\mathcal{L}\phi, \phi) + (g, 1), \tag{6}$$

where  $\mathcal{L}$  is a linear, self-adjoint operator, and g is a potential functional that might depend on  $\phi$  and its low order spatial derivatives. For instance, given the Ginzburg–Landau free energy functional for the two phase immersible materials

$$F = \int_{\Omega} \gamma \left[ \frac{\varepsilon}{2} |\nabla \phi|^2 + \frac{1}{\varepsilon} \phi^2 (1 - \phi)^2 \right] d\mathbf{x},\tag{7}$$

where  $\gamma$  is the surface tension, and  $\varepsilon$  is the interfacial thickness, we recast

$$\mathcal{L} = -\gamma \varepsilon \Delta + \gamma_0, \quad g(\phi) = \frac{\gamma}{\varepsilon} \phi^2 (1 - \phi)^2 - \frac{\gamma_0}{2} \phi^2, \tag{8}$$

where  $\gamma_0$  is a non-negative constant (regularization parameter [9]). We assume periodic boundary conditions throughout the study.

Gradient flow model (5) can be rewritten as

$$\partial_t \phi = \mathcal{G} \left( \mathcal{L} \phi + \frac{\delta g}{\delta \phi} \right). \tag{9}$$

Note that if  $\mathcal L$  is self-adjoint and  $\mathcal G$  is negative semi-definite, we have

$$(\mathcal{L}\phi, \psi) = (\phi, \mathcal{L}\psi), \quad (\psi, \mathcal{G}\psi) \le 0, \quad \forall \phi, \psi \in L^2(\Omega).$$
 (10)

Therefore, the gradient flow system (9) satisfies the following energy dissipation law

$$\frac{dF}{dt} = \left(\mathcal{L}\phi + \frac{\delta g}{\delta \phi}, \partial_t \phi\right) = \left(\mathcal{L}\phi + \frac{\delta g}{\delta \phi}, \mathcal{G}(\mathcal{L}\phi + \frac{\delta g}{\delta \phi})\right) \le 0. \tag{11}$$

#### 2.2. Model reformulation using the SAV approach

For simplicity, we assume g only depends on  $\phi$ , not its spatial derivatives. We note that the SAV approach works for a more general g. We first introduce a scalar auxiliary variable (SAV)

$$q(t) = \sqrt{(g(\phi), 1) + C_0},$$
 (12)

where  $C_0$  is a positive number such that  $(g(\phi), 1) + C_0 > 0$ . Then we reformulate the original gradient flow system (9) into the following equivalent PDEs

$$\begin{cases} \partial_t \phi = \mathcal{G}\left(\mathcal{L}\phi + \frac{qg'(\phi)}{\sqrt{\left(g(\phi),1\right) + C_0}}\right), \\ \frac{d}{dt}q = \left(\frac{g'(\phi)}{2\sqrt{\left(g(\phi),1\right) + C_0}}, \ \partial_t \phi\right), \end{cases}$$
(13)

with consistent initial condition

$$q|_{t=0} = \sqrt{(g(\phi|_{t=0}), 1) + C_0}.$$
 (14)

It is obvious that (13) along with consistent initial condition (14) is equivalent to the original gradient flow system given in (9). We then shift our focus to design arbitrarily high-order numerical approximations for equivalent model (13).

In reformulated system (13), the reformulated free energy is given by

$$E = \frac{1}{2}(\mathcal{L}\phi, \phi) + q^2 - C_0, \tag{15}$$

which is equal to free energy F of the original system (9) in the continuous level. System (13) satisfies the reformulated energy dissipation law

$$\frac{dE}{dt} = (\mathcal{L}\phi, \phi_t) + 2q \frac{dq}{dt} = \left(\mathcal{L}\phi + \frac{qg'(\phi)}{\sqrt{(g(\phi), 1) + C_0}}, \phi_t\right)$$

$$= \left(\mathcal{L}\phi + \frac{qg'(\phi)}{\sqrt{(g(\phi), 1) + C_0}}, G(\phi)\right)$$

$$\mathcal{G}\left(\mathcal{L}\phi + \frac{qg'(\phi)}{\sqrt{(g(\phi), 1) + C_0}}\right) \le 0. \tag{16}$$

Next we will develop arbitrarily high-order unconditionally energy stable numerical approximations to SAV reformulated system (13)-(14).

#### 3. High order time discretization

In this section, we derive classes of RK methods and collocation methods in time for SAV reformulated system (13), respectively. Then, we show that both the classes of RK methods and collocation methods with the Gaussian quadrature nodes preserve the corresponding energy dissipation law and thus are unconditionally energy stable.

Applying a s-stage RK method to system (13), we obtain the following HSAV-RK scheme.

**Scheme 3.1** (s-stage HSAV-RK Method). Let  $b_i$ ,  $a_{ij}$  (i, j = 1, ..., s) be real numbers and let  $c_i = \sum_{j=1}^s a_{ij}$ . For given  $(\phi^n, q^n)$ , the following intermediate values are first calculated by

$$\Phi_{i} = \phi^{n} + \Delta t \sum_{j=1}^{s} a_{ij} k_{j},$$

$$Q_{i} = q^{n} + \Delta t \sum_{j=1}^{s} a_{ij} l_{j},$$

$$k_{i} = \mathcal{G} \left( \mathcal{L} \Phi_{i} + \frac{Q_{i} g'(\Phi_{i})}{\sqrt{\left(g(\Phi_{i}), 1\right) + C_{0}}} \right),$$

$$l_{i} = \left( \frac{g'(\Phi_{i})}{2\sqrt{\left(g(\Phi_{i}), 1\right) + C_{0}}}, k_{i} \right).$$
(17)

Then  $(\phi^{n+1}, q^{n+1})$  is updated via

$$\phi^{n+1} = \phi^n + \Delta t \sum_{i=1}^{s} b_i k_i,$$

$$q^{n+1} = q^n + \Delta t \sum_{i=1}^{s} b_i l_i.$$
(18)

The RK coefficients are usually displayed by a Butcher table

$$\frac{\mathbf{c} \mid \mathbf{A}}{\mid \mathbf{b}^{T}} = \frac{\begin{array}{c|cccc} c_{1} & a_{11} & \cdots & a_{1s} \\ \vdots & \vdots & & \vdots \\ c_{s} & a_{s1} & \cdots & a_{ss} \\ \hline & b_{1} & \cdots & b_{r} \end{array}}{,}$$

where  $\mathbf{A} \in \mathbb{R}^{s \times s}$ ,  $\mathbf{b} \in \mathbb{R}^{s}$ , and  $\mathbf{c} = \mathbf{A}\mathbf{l}$  with  $\mathbf{l} = (1, 1, ..., 1)^{T} \in \mathbb{R}^{s}$ . For general HSAV-RK methods, we have the following theorem for the energy-stability.

**Theorem 3.1.** If the coefficients of an HSAV-RK method satisfy

$$b_i a_{ii} + b_i a_{ii} = b_i b_i, \quad b_i \ge 0, \quad \forall i, j = 1, \dots, s,$$
 (19)

then it is unconditionally energy stable, i.e., it satisfies the following energy dissipation law

$$E^{n+1} - E^n = \Delta t \sum_{i=1}^s b_i \left( \mathcal{L} \Phi_i + \frac{Q_i g'(\Phi_i)}{\sqrt{\left(g(\Phi_i), 1\right) + C_0}}, \right.$$

$$\mathcal{G} \left[ \mathcal{L} \Phi_i + \frac{Q_i g'(\Phi_i)}{\sqrt{\left(g(\Phi_i), 1\right) + C_0}} \right] \right) \le 0, \tag{20}$$

where  $E^n = \frac{1}{2}(\mathcal{L}\phi^n, \phi^n) + (q^n)^2 - C_0$ .

**Proof.** Denoting  $\phi^{n+1} = \phi^n + \Delta t \sum_{i=1}^s b_i k_i$  and noticing that the operator  $\mathcal{L}$  is linear and self-adjoint, we have

$$\frac{1}{2}(\mathcal{L}\phi^{n+1}, \phi^{n+1}) - \frac{1}{2}(\mathcal{L}\phi^{n}, \phi^{n}) 
= \Delta t \sum_{i=1}^{s} b_{i}(k_{i}, \mathcal{L}\phi^{n}) + \frac{\Delta t^{2}}{2} \sum_{i,j=1}^{s} b_{i}b_{j}(k_{i}, \mathcal{L}k_{j}).$$
(21)

Applying  $\phi^n = \Phi_i - \Delta t \sum_{j=1}^s a_{ij} k_j$  to the right hand side of (21), we deduce

$$\frac{1}{2}(\mathcal{L}\phi^{n+1},\phi^{n+1}) - \frac{1}{2}(\mathcal{L}\phi^{n},\phi^{n}) = \Delta t \sum_{i=1}^{s} b_{i}(k_{i},\mathcal{L}\Phi_{i}),$$
 (22)

where  $\sum_{i,j=1}^{s} b_i a_{ij}(k_i, \mathcal{L}k_j) = \sum_{i,j=1}^{s} b_j a_{ji}(k_i, \mathcal{L}k_j)$  and  $b_i a_{ij} + b_j a_{ji} = b_i b_j$  were used. Similarly, we have

$$|q^{n+1}|^2 - |q^n|^2 = 2\Delta t \sum_{i=1}^s b_i l_i Q_i = \Delta t \sum_{i=1}^s b_i \left( \frac{Q_i g'(\Phi_i)}{\sqrt{(g(\Phi_i), 1) + C_0}}, k_i \right).$$
 (23)

Adding (22) and (23) leads to

$$E^{n+1} - E^n = \Delta t \sum_{i=1}^{s} b_i \left( \mathcal{L} \Phi_i + \frac{Q_i g'(\Phi_i)}{\sqrt{\left( g(\Phi_i), 1 \right) + C_0}}, k_i \right). \tag{24}$$

Substituting 
$$k_i = \mathcal{G}\left(\mathcal{L}\Phi_i + \frac{Q_ig'(\Phi_i)}{\sqrt{\left(g(\Phi_i),1\right) + C_0}}\right)$$
 in (24), we arrive at (20). This completes the proof.  $\square$ 

Applying an *s*-stage collocation method to system (13), we obtain the following HSAV-Collocation scheme.

**Scheme 3.2** (s-stage HSAV Collocation Method). Let  $c_1, \ldots, c_s$  be distinct real numbers  $(0 \le c_i \le 1)$ . For given  $(\phi^n, q^n)$ , the collocation polynomials u(t) and v(t) are two polynomials of degree s satisfying

$$u(t_n) = \phi^n, \quad v(t_n) = q^n, \tag{25}$$

$$\partial_t u(t_n^i) = \mathcal{G}\left(\mathcal{L}u(t_n^i) + \frac{v(t_n^i)g'(u(t_n^i))}{\sqrt{\left(g(u(t_n^i)), 1\right) + C_0}}\right),\tag{26}$$

$$\partial_t v(t_n^i) = \left(\frac{g'\left(u(t_n^i)\right)}{2\sqrt{\left(g\left(u(t_n^i)\right), 1\right) + C_0}}, \, \partial_t u(t_n^i)\right),\tag{27}$$

where  $t_n^i = t_n + c_i \Delta t$  and i = 1, ..., s. And then the numerical solution is defined by  $\phi^{n+1} = u(t_n + \Delta t)$  and  $q^{n+1} = v(t_n + \Delta t)$ .

Theorem 1.4 on page 31 of [38] indicates that the collocation method yields a special RK method. If the collocation points  $c_1, \ldots, c_s$  are chosen as Gaussian quadrature nodes, i.e., the zeros of the sth shifted Legendre polynomial  $\frac{d^s}{dx^s} \left( x^s (x-1)^s \right)$ , Scheme 3.2 is called the Gaussian collocation method. Based on the Gaussian quadrature nodes, the interpolating quadrature formula has order 2s, and the Gaussian collocation method shares the same order 2s. For instance, the RK coefficients of fourth order and sixth order HSAV schemes are given explicitly in Table 1 (see [38] for coefficients of higher orders).

For conservative systems with quadratic invariants, the Gaussian collocation methods have been proven to conserve the corresponding discrete quadratic invariants [38]. Here we show that these translate into unconditionally energy stability for the SAV reformulated system (13).

**Theorem 3.2.** The s-stage HSAV Gaussian collocation Scheme 3.2 is unconditionally energy stable, i.e., it satisfies the following energy dissipation law

$$E^{n+1} - E^{n}$$

$$= \Delta t \sum_{i=1}^{s} b_{i} \left( \mathcal{L}u(t_{n}^{i}) + \frac{v(t_{n}^{i})g'(u(t_{n}^{i}))}{\sqrt{\left(g(u(t_{n}^{i})), 1\right) + C_{0}}}, \right.$$

$$\mathcal{G}\left[ \mathcal{L}u(t_{n}^{i}) + \frac{v(t_{n}^{i})g'(u(t_{n}^{i}))}{\sqrt{\left(g(u(t_{n}^{i})), 1\right) + C_{0}}} \right] \right)$$

$$\leq 0, \tag{28}$$

where  $E^n=\frac{1}{2}(\mathcal{L}\phi^n,\phi^n)+(q^n)^2-C_0$  and  $t^i_n=t_n+c_i\Delta t,\ c_i$   $(i=1,\ldots,s)$  are the Gaussian quadrature nodes,  $b_i\geq 0$   $(i=1,\ldots,s)$  are the Gauss–Legendre quadrature weights, u(t),v(t) are the collocation polynomials of the Gaussian collocation methods.

**Proof.** Noticing  $\phi^n = u(t_n)$ ,  $q^n = v(t_n)$  and  $\phi^{n+1} = u(t_{n+1})$ ,  $q^{n+1} = v(t_{n+1})$ , we have

$$\begin{split} E^{n+1} - E^n &= \frac{1}{2} (\mathcal{L}\phi^{n+1}, \phi^{n+1}) - \frac{1}{2} (\mathcal{L}\phi^n, \phi^n) + (q^{n+1})^2 - (q^n)^2 \\ &= \frac{1}{2} (u(t_{n+1}), \mathcal{L}u(t_{n+1})) - \frac{1}{2} (u(t_n), \mathcal{L}u(t_n)) \\ &+ |v(t_{n+1})|^2 - |v(t_n)|^2 \\ &= \int_{t_n}^{t_{n+1}} \left[ \frac{1}{2} \frac{d}{dt} (u(t), \mathcal{L}u(t)) + \frac{d}{dt} |v(t)|^2 \right] dt \\ &= \int_{t_n}^{t_{n+1}} \left[ (\dot{u}(t), \mathcal{L}u(t)) + 2\dot{v}(t)v(t) \right] dt. \end{split}$$

The integrand  $(\dot{u}(t), \mathcal{L}u(t))$  and  $\dot{v}(t)v(t)$  are polynomial of degree 2s-1, which is integrated without error by the s-stage Gaussian quadrature formula. It therefore follows from the collocation condition that

$$\begin{split} &\int_{t_n}^{t_{n+1}} \left[ \left( \dot{u}(t), \mathcal{L}u(t) \right) + 2\dot{v}(t)v(t) \right] dt \\ &= \Delta t \sum_{i=1}^{s} b_i \left[ \left( \dot{u}(t_n^i), \mathcal{L}u(t_n^i) \right) + 2\dot{v}(t_n^i)v(t_n^i) \right] \\ &= \Delta t \sum_{i=1}^{s} b_i \left( \dot{u}(t_n^i), \mathcal{L}u(t_n^i) + \frac{v(t_n^i)g'\left(u(t_n^i)\right)}{\sqrt{\left(g\left(u(t_n^i)\right), 1\right) + C_0}} \right) \\ &= \Delta t \sum_{i=1}^{s} b_i \left( \mathcal{L}u(t_n^i) + \frac{v(t_n^i)g'\left(u(t_n^i)\right)}{\sqrt{\left(g\left(u(t_n^i)\right), 1\right) + C_0}}, \right. \\ &\mathcal{G} \left[ \mathcal{L}u(t_n^i) + \frac{v(t_n^i)g'\left(u(t_n^i)\right)}{\sqrt{\left(g\left(u(t_n^i)\right), 1\right) + C_0}} \right] \right) \leq 0, \end{split}$$

which leads to (28). This completes the proof.  $\Box$ 

**Remark 3.1.** The proposed high-order energy stable schemes do not depend on the specific form of mobility  $\mathcal{G}$  and free energy F so that they work for any gradient flow models (5).

**Remark 3.2.** Due to the collocation method reduces to a special RK method, we have to solve the nonlinear system (17), which can be implemented by using a simple fixed-point iteration method. Please see [37] for more details. At each time step, even though solving an HSAV scheme takes longer than solving the SAV scheme, much larger time step size can be used for the HSAV scheme than the low order SAV schemes to reach the same accuracy (due to the high-order accuracy of the HSAV scheme). Overall, for simulations reaching similar accuracy, the HSAV scheme will take less CPU time than the low order SAV schemes, making the HSAV scheme very competitive for long time dynamic simulations.

#### 4. Spatial discretization

To make the order of accuracy in space compatible with the arbitrarily high-order in time, we employ the Fourier pseudospectral method in space for Schemes 3.1 and 3.2 to arrive at fully discrete HSAV-RK schemes and fully discrete HSAV collocation schemes, respectively. Then, we show the fully discrete HSAV-RK scheme with (19) and the fully discrete HSAV Gaussian collocation scheme to preserve the corresponding energy dissipation law in the fully discrete level.

To make the paper self-explanatory, we briefly reintroduce the following notations (see [39,40] for more details). Let  $N_x$ ,  $N_y$  be two positive even integers. Domain  $\Omega = [0, L_x] \times [0, L_y]$  is uniformly partitioned with mesh size  $h_x = L_x/N_x$ ,  $h_y = L_y/N_y$  and

$$\Omega_h = \{ (x_j, y_k) | x_j = jh_x, y_k = kh_y,$$

$$0 \le j \le N_x - 1, 0 \le k \le N_y - 1 \}.$$

Let  $V_h = \{u|u = \{u_{j,k}|(x_j, y_k) \in \Omega_h\}\}$  be the space of grid functions on  $\Omega_h$ . For any two vector grid functions  $\mathbf{u} = (u_m), \mathbf{v} = (v_m)$   $(u_m, v_m \in V_h)$ , we define the discrete inner product and norm as follows

$$(\mathbf{u}, \mathbf{v})_h = h_x h_y \sum_m \sum_{j=0}^{N_x-1} \sum_{k=0}^{N_y-1} (u_m)_{j,k} (v_m)_{j,k}, \quad \|\mathbf{u}\|_h = \sqrt{(\mathbf{u}, \mathbf{u})_h}.$$

Table 1

RK coefficients of Gaussian collocation methods of order 4 and 6.

We denote

$$S_N = \text{span}\{X_j(x)Y_k(y), j = 0, 1, \dots, N_x - 1; k = 0, 1, \dots, N_y - 1\}$$

as the interpolation space, where  $X_j(x)$  and  $Y_k(y)$  are trigonometric polynomials of degree  $N_x/2$  and  $N_y/2$ , given respectively by

$$X_{j}(x) = \frac{1}{N_{x}} \sum_{m=-N_{x}/2}^{N_{x}/2} \frac{1}{a_{m}} e^{im\mu_{x}(x-x_{j})},$$
 (29)

$$Y_k(y) = \frac{1}{N_y} \sum_{m = -N_y/2}^{N_y/2} \frac{1}{b_m} e^{im\mu_y(y - y_k)},$$
(30)

where

$$a_m = \begin{cases} 1, |m| < N_x/2, \\ 2, |m| = N_x/2, \end{cases} \quad b_m = \begin{cases} 1, |m| < N_y/2, \\ 2, |m| = N_y/2, \end{cases}$$

and  $\mu_X = 2\pi/L_X$ ,  $\mu_Y = 2\pi/L_Y$ . We define the interpolation operator  $I_N : C(\Omega) \to S_N$  as follows:

$$I_N u(x, y) = \sum_{j=0}^{N_X - 1} \sum_{k=0}^{N_Y - 1} u_{j,k} X_j(x) Y_k(y),$$
(31)

where  $u_{j,k} = u(x_j, y_k)$ . Then, we differentiate (31) and evaluate the resulting expressions at point  $(x_j, y_k)$  as follows

$$\partial_x^{s_1} \partial_y^{s_2} I_N u(x_j, y_k) = \sum_{m_1=0}^{N_x-1} \sum_{m_2=0}^{N_y-1} u_{m_1, m_2} (\mathbf{D}_{s_1}^x)_{j, m_1} (\mathbf{D}_{s_2}^y)_{k, m_2},$$

where  $\mathbf{D}_{s_1}^{x}$  and  $\mathbf{D}_{s_2}^{y}$  are  $N_x \times N_x$  and  $N_y \times N_y$  matrices, respectively, with elements given by

$$(\mathbf{D}_{s_1}^{\mathsf{x}})_{j,m} = \frac{d^{s_1} X_m(x_j)}{dx^{s_1}}, \ (\mathbf{D}_{s_2}^{\mathsf{y}})_{k,m} = \frac{d^{s_2} Y_m(y_k)}{dy^{s_2}}.$$

Define three operators  $\odot$ ,  $\otimes$  and  $\odot$  as follows:

$$(u \odot v)_{j,k} = u_{j,k}v_{j,k}, \ (\mathbf{A} \otimes u)_{j,k} = \sum_{m=0}^{N_x-1} \mathbf{A}_{j,m}u_{m,k},$$

$$(\mathbf{B} \odot u)_{j,k} = \sum_{m=0}^{N_y-1} \mathbf{B}_{k,m} u_{j,m},$$

where  $u, v \in V_h$ . It is easy to show that these three operators possess the following properties:

$$u\odot v=v\odot u,\ \mathbf{A}\otimes\mathbf{B}\odot u=\mathbf{B}\odot\mathbf{A}\otimes u,\ \mathbf{A}@\mathbf{B}@u=(\mathbf{A}\mathbf{B})@u,$$
 @  $=\otimes$  or  $\odot$ .

Then we have

$$\partial_x^{s_1}\partial_y^{s_2}I_Nu(x_j,y_k)=(\mathbf{D}_{s_1}^x\otimes\mathbf{D}_{s_2}^y\otimes u)_{j,k}.$$

Lemma 4.1 ([41]). Denote

$$\boldsymbol{\varLambda}_{\alpha,s} = \left\{ \begin{array}{l} \left[i\mu_{\alpha} diag\left(0,1,\ldots,\frac{N_{\alpha}}{2}-1,0,-\frac{N_{\alpha}}{2}+1,\ldots,-1\right)\right]^{s},\\ when s odd,\\ \left[i\mu_{\alpha} diag\left(0,1,\ldots,\frac{N_{\alpha}}{2}-1,\frac{N_{\alpha}}{2},-\frac{N_{\alpha}}{2}+1,\ldots,-1\right)\right]^{s},\\ when s even,\\ \boldsymbol{\alpha} = x \text{ or } v. \end{array} \right.$$

we have

$$\mathbf{D}_{s}^{\alpha} = F_{N_{\alpha}}^{-1} \Lambda_{\alpha,s} F_{N_{\alpha}},\tag{32}$$

where  $F_{N_{\alpha}}$  is the discrete Fourier transform, and  $F_{N_{\alpha}}^{-1}$  is the discrete inverse Fourier transform.

**Lemma 4.2.** For real matrix  $\mathbf{A} \in \mathbb{R}_{N_a \times N_a}$ , a = x or y, and  $u, v \in V_h$ ,

$$(\mathbf{A}(\mathbf{a})u, v)_h = (u, \mathbf{A}^T(\mathbf{a})v)_h. \tag{33}$$

Using identity (33), anti-symmetry of  $\mathbf{D}_{2s-1}^{a}$  and symmetry of  $\mathbf{D}_{2s}^{a}$ ,  $\forall a \in \{x, y\}, s \in \mathbb{Z}^{+}$ , we obtain

$$\begin{pmatrix} \mathbf{D}_{2s-1}^{\mathbf{a}} @ u, v \end{pmatrix}_{h} = -\left(u, \mathbf{D}_{2s-1}^{\mathbf{a}} @ v\right)_{h}, 
\left(\mathbf{D}_{2s}^{\mathbf{a}} @ u, v\right)_{h} = \left(u, \mathbf{D}_{2s}^{\mathbf{a}} @ v\right)_{h},$$

which implies that the Fourier pseudospectral method preserves discrete integration-by-parts formulae. Therefore, we apply the Fourier pseudospectral method in space to obtain the corresponding discrete self-adjoint operator  $\mathcal{L}_h$  and the negative semi-definite operator  $\mathcal{G}_h$ , i.e.,

$$(\mathcal{L}_h \phi, \psi)_h = (\phi, \mathcal{L}_h \psi)_h, \quad (\psi, \mathcal{G}_h \psi)_h \le 0, \quad \forall \phi, \psi \in V_h. \tag{34}$$

Applying the Fourier pseudospectral method to Scheme 3.1, we obtain the following fully discrete scheme.

**Scheme 4.1** (Fully Discrete HSAV-RK Method). Let  $b_i$ ,  $a_{ij}$  (i, j = 1, ..., s) be real numbers and let  $c_i = \sum_{j=1}^s a_{ij}$ . For given  $\phi^n \in V_h$  and  $q^n \in \mathbb{R}$ , the following intermediate values are first calculated by

$$\Phi_{i} = \phi^{n} + \Delta t \sum_{j=1}^{s} a_{ij}k_{j},$$

$$Q_{i} = q^{n} + \Delta t \sum_{j=1}^{s} a_{ij}l_{j},$$

$$k_{i} = \mathcal{G}_{h} \left( \mathcal{L}_{h}\Phi_{i} + \frac{Q_{i}g'(\Phi_{i})}{\sqrt{\left(g(\Phi_{i}),1\right)_{h} + C_{0}}} \right),$$

$$l_{i} = \left( \frac{g'(\Phi_{i})}{2\sqrt{\left(g(\Phi_{i}),1\right)_{h} + C_{0}}}, k_{i} \right),$$
(35)

where  $\Phi_i$ ,  $k_i \in V_h$ ,  $Q_i$ ,  $l_i \in \mathbb{R}$ . Then  $\phi^{n+1} \in V_h$ ,  $q^{n+1} \in \mathbb{R}$  is updated via

$$\phi^{n+1} = \phi^n + \Delta t \sum_{i=1}^{s} b_i k_i,$$

$$q^{n+1} = q^n + \Delta t \sum_{i=1}^{s} b_i l_i.$$
(36)

Applying the Fourier pseudospectral method to Scheme 3.2, we obtain the following fully discrete scheme.

**Scheme 4.2** (Fully Discrete HSAV Collocation Method). Let  $c_1, \ldots, c_s$  be distinct real numbers  $(0 \le c_i \le 1)$ . For given  $\phi^n \in V_h$  and  $q^n \in \mathbb{R}$ , u(t) is a  $N_x \times N_y$  matrix polynomial of degree s and v(t) is a polynomial of degree s satisfying

$$u(t_n) = \phi^n, \quad v(t_n) = q^n, \tag{37}$$

$$\dot{u}(t_n^i) = \mathcal{G}_h \left( \mathcal{L}_h u(t_n^i) + \frac{v(t_n^i)g'(u(t_n^i))}{\sqrt{\left(g(u(t_n^i)), 1\right)_h + C_0}} \right), \tag{38}$$

$$\dot{v}(t_n^i) = \left(\frac{g'(u(t_n^i))}{2\sqrt{\left(g(u(t_n^i)), 1\right)_h + C_0}}, \dot{u}(t_n^i)\right)_h, \tag{39}$$

where  $t_n^i = t_n + c_i \Delta t$  and i = 1, ..., s. And then the numerical solution is defined by  $\phi^{n+1} = u(t_n + \Delta t)$  and  $q^{n+1} = v(t_n + \Delta t)$ .

Analogous to the semidiscrete schemes, we have the following theorems for the fully discrete schemes.

**Theorem 4.1.** If the coefficients of a fully discrete HSAV-RK method satisfy

$$b_i a_{ij} + b_j a_{ji} = b_i b_j, \quad b_i \ge 0, \quad \forall i, j = 1, \dots, s,$$
 (40)

then it is unconditionally energy stable, i.e., it satisfies the following energy dissipation law

$$E_h^{n+1} - E_h^n = \Delta t \sum_{i=1}^s b_i \left( \mathcal{L}_h \Phi_i + \frac{Q_i g'(\Phi_i)}{\sqrt{\left( g(\Phi_i), 1 \right)_h + C_0}}, \right.$$

$$\mathcal{G}_h \left[ \mathcal{L}_h \Phi_i + \frac{Q_i g'(\Phi_i)}{\sqrt{\left( g(\Phi_i), 1 \right)_h + C_0}} \right] \right)_h \le 0, \tag{41}$$

where  $E_h^n = \frac{1}{2} (\mathcal{L}_h \phi^n, \phi^n)_h + (q^n)^2 - C_0$ .

**Theorem 4.2.** The fully discrete HSAV Gaussian collocation Scheme 4.2 is unconditionally energy stable, i.e., it satisfies the following energy dissipation law

$$E_{h}^{n+1} - E_{h}^{n}$$

$$= \Delta t \sum_{i=1}^{s} b_{i} \left( \mathcal{L}_{h} u(t_{n}^{i}) + \frac{v(t_{n}^{i}) g'(u(t_{n}^{i}))}{\sqrt{\left(g(u(t_{n}^{i})), 1\right)_{h} + C_{0}}}, \right.$$

$$\mathcal{G}_{h} \left[ \mathcal{L}_{h} u(t_{n}^{i}) + \frac{v(t_{n}^{i}) g'(u(t_{n}^{i}))}{\sqrt{\left(g(u(t_{n}^{i})), 1\right)_{h} + C_{0}}} \right] \right)_{h}$$

$$\leq 0.$$
(42)

$$\leq 0,$$
 (42)

where  $E_h^n=\frac{1}{2}(\mathcal{L}_h\phi^n,\phi^n)_h+(q^n)^2-C_0$  and  $t_n^i=t_n+c_i\Delta t,\,c_i\,(i=1,\ldots,s)$  are the Gaussian quadrature nodes,  $b_i\geq 0\,(i=1,\ldots,s)$  are the Gauss–Legendre quadrature weights.

**Remark 4.1.** As the proofs of Theorems 4.1 and 4.2 are similar to their semi-discrete counterparts in Theorems 3.1 and 3.2, we omit the details. It is worth mentioning that the proposed schemes only satisfy the modified energy dissipation law in the discrete form of (15), instead of the original energy in (6). However, we note that the discrete version of (15) is a high-order approximation of (6).

**Remark 4.2.** In general, the energy decay often implies that the numerical solution is bounded in the energy norm. In this regard, the HSAV schemes possess a good nonlinear stability, which is also known as energy stability. However, it does not necessarily mean that the numerical solution is bounded in  $L^{\infty}$  norm. In Ref. [42], Tang et al. proposed a class of implicit–explicit schemes for the Allen–Cahn equation, which could preserve the maximal principle and satisfy the discrete energy stability. Since the proposed schemes in this paper are fully implicit and nonlinear, it is very difficult to prove that our schemes satisfy the maximal principle. How to develop high-order numerical methods that preserve the maximum principle will be considered in our further work

#### 5. Numerical results

In this section, we conduct three numerical tests to benchmark the theoretical results. We reiterate that the newly proposed HSAV schemes can reach arbitrarily high order accuracy in time (with a proper choice of the Gaussian collocation points), and they are all unconditionally energy stable. For simplicity, we only test the 4th and 6th order scheme for the demonstration purpose. Moreover, the CPU time is calculated with a 3.2 GHz Intel Core i7 using Matlab R2018b on MacOS Mojave version 10.14.2.

**Example 1** (*Allen–Cahn Equation*). First of all, we test the proposed numerical schemes for solving the Allen–Cahn (AC) equation [6]:

$$\partial_t \phi = -M \Big( -\varepsilon^2 \Delta \phi + (\phi^3 - \phi) \Big), \tag{43}$$

where M is the mobility parameter and  $\varepsilon$  controls the interfacial thickness. We choose the benchmark problem given in [43], i.e. set the initial profile of  $\phi$  as

$$\phi(x, y, 0) = \begin{cases} 1, & x^2 + y^2 < 100^2, \\ -1, & x^2 + y^2 \ge 100^2, \end{cases}$$
 (44)

which is a disk centered at the origin, and use domain  $\Omega = [-128, 128]^2$ . The parameters are chosen as  $M = \varepsilon = 1$ . It is known that the area of the disk will shrink, following the scaling law  $V = \pi R_0^2 - 2\pi t$  asymptotically, where  $R_0$  is the initial radius. Here we test the dynamics using the proposed HSAV schemes. The numerical results are summarized in Fig. 1. We observe that the HSAV schemes can use much larger time steps to capture the correct volume shrinking dynamics than the low order SAV schemes.

**Example 2** (*Cahn–Hilliard Equation*). Next, we study the Cahn–Hilliard equation with a Ginzburg–Landau free energy. Specifically, given Ginzburg–Landau free energy  $F=(-\frac{\varepsilon^2}{2}\Delta\phi,\phi)+(\frac{1}{4}(1-\phi^2)^2,1)$  and constant mobility  $\lambda$ , the model is proposed as

$$\partial_t \phi = \lambda \Delta \left[ -\varepsilon^2 \Delta \phi + (\phi^3 - \phi) \right]. \tag{45}$$

If we set  $\mathcal{G}=\lambda\Delta$ ,  $\mathcal{L}=-\varepsilon^2\Delta+\gamma_0$  and  $g(\phi)=\frac{1}{4}(1-\phi^2)^2-\frac{\gamma_0}{2}\phi^2+\frac{\zeta_0}{|\Omega|}$ , where  $C_0$  is a constant such that (g,1)>0. By

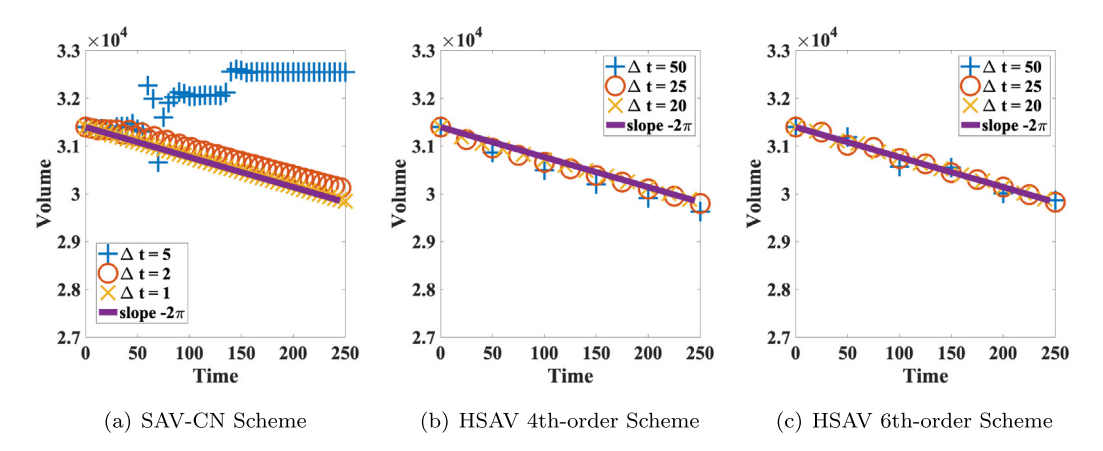
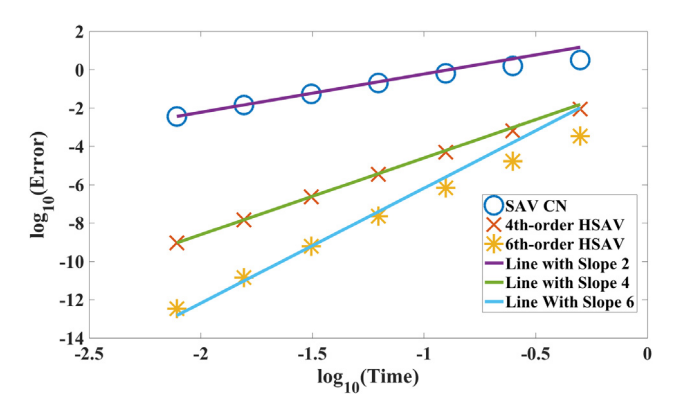


Fig. 1. Benchmark problem for disk shrinking using the Allen–Cahn equation. This figure shows the area of a disk shrinks in time with different schemes and various time steps. The second order SAV scheme based on the Crank–Nicolson method, the fourth and sixth order RK schemes are displayed. The high order RK methods can produce the correct scaling rate at much large time steps than the low order CN scheme.



**Fig. 2.** Time step refinement test for the SAV schemes for the Cahn-Hilliard equation. This figure demonstrates the HSAV schemes can reach their expected high-order accuracy. Their numerical errors are much smaller than that of the SAV-CN scheme.

introducing the scalar auxiliary variable  $q = \sqrt{(g,1)}$ , the Cahn-Hilliard equation (45) can be rewritten as the reformulated form of (13)

$$\partial_t \phi = \lambda \Delta \left[ -\varepsilon^2 \Delta \phi + \gamma_0 \phi + \frac{q}{\sqrt{(g,1)}} g' \right],$$

$$\frac{d}{dt} q = \left( \frac{g'}{2\sqrt{(g,1)}}, \partial_t \phi \right),$$
(46)

with the consistent initial condition for q:  $q(t = 0) = \sqrt{(g, 1)}|_{t=0}$ .

First of all, we conduct a time-step refinement test to verify the accuracy of the proposed schemes. We choose the domain as  $\Omega=[0,1]\times[0,1]$  and spatial meshes  $N_x=N_y=256$ . The parameters are chosen as  $\lambda=10^{-3}$ ,  $\varepsilon=0.01$ ,  $\gamma_0=1$ ,  $C_0=1$ . The initial profile for  $\phi$  is given as  $\phi(x,y,0)=\sin(2\pi x)\sin(2\pi y)$ . Both the SAV Crank–Nicolson (SAV-CN) scheme (see [5]) and the newly proposed HSAV Scheme 3.2 with fourth order and sixth order collocation points are tested. The numerical errors in  $L^2$  norm at t=1 are summarized in Fig. 2. We observe that the two HSAV schemes reach the fourth and sixth order accuracy respectively. In particular, the  $L^2$  errors of HSAV schemes are significantly (in several orders of magnitudes) smaller than the SAV-CN scheme.

In addition, to assure the  $L^2$  norm of the numerical error for  $\phi$  at t=1 smaller than  $10^{-10}$ , the approximate time steps are  $\Delta t=10^{-5}$  for the SAV-CN scheme,  $\Delta t=0.004$  for the HSAV 4th-order scheme,  $\Delta t=0.02$  for the HSAV 6th-order scheme. The total CPU time is summarized in Table 2, where we observe the

**Table 2**Total CPU time using various numerical schemes solving the CH model.

	SAV-CN scheme	HSAV 4th-order scheme	HSAV 6th-order scheme
$\Delta t$ CPU time (seconds)	0.00001	0.025	0.02
	165.32	3.00	2.62

HSAV schemes take much less CPU time than the SAV-CN scheme to achieve the same accuracy. It indicates the HSAV schemes are superior to the SAV-CN scheme for accurate long-time dynamic simulations.

Next we compare the different SAV schemes for simulating coarsening dynamics of a binary immersible fluid using the Cahn–Hilliard equation in (45). We choose the domain as  $\Omega = [0, 4\pi] \times [0, 4\pi]$  and meshes  $N_x = N_y = 512$ . The parameters are chosen as  $\lambda = 0.1$ ,  $\varepsilon = 0.025$ ,  $\gamma_0 = 1$ ,  $C_0 = 1$ . We use an initial profile of  $\phi$  as

$$\phi(x, y, 0) = 0.001 \text{rand}(x, y). \tag{47}$$

where  $\operatorname{rand}(x,y)$  generates random number between -1 and 1. The predicted energy evolution using different SAV schemes with various time steps are summarized in Fig. 3. We observe that for the SAV-CN scheme, it can predict the correct energy evolution with time step  $\Delta t = 0.00025$  (where the predicted energy evolution with time step  $\Delta t = 0.0005$  is noticeably inaccurate). For the fourth order HSAV scheme, it can predict accurate energy evolution even with time step  $\Delta t = 0.05$ ; and for the sixth order HSAV scheme, it even works well with time step  $\Delta t = 0.1$ , which is more than  $10^3$  larger than the one with the SAV-CN scheme.

Then we use the HSAV schemes to conduct the long-time dynamic simulations of coarsening. We use the same parameters as above, and choose the initial profile

$$\phi(x, y, 0) = \phi_0 + 0.001 \text{rand}(x, y), \tag{48}$$

where  $\phi_0$  is a constant and rand(x,y) generates a random number in the range of -1 to 1. Then we choose  $\phi_0=0,0.1,0.5$ . We use the sixth order HSAV scheme with time step  $\Delta t=0.1$ . The simulation results are summarized in Fig. 4, where we present the profile of  $\phi$  at different times. We can observe the HSAV schemes can capture the phase transition dynamics accurately even with such a large time step time size. In particular, when  $\phi_0$  is small, i.e., the two components have similar total volume, the spinodal decomposition takes effect. When the volume of one phase is dominant, (for instance,  $\phi_0=0.5$ ), the nucleation takes effects. These results are in a strong agreement with reports in [44].

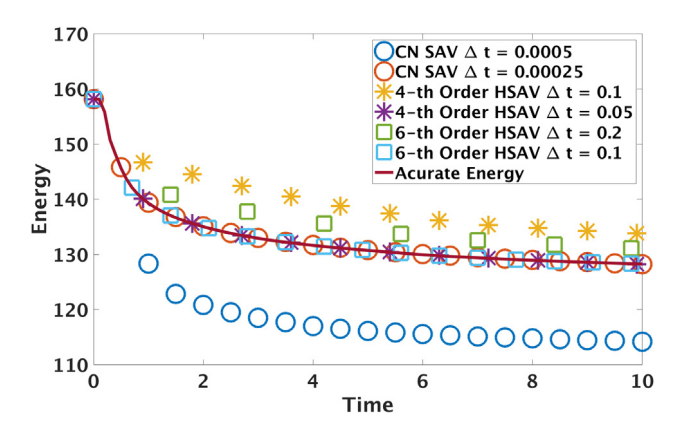


**Fig. 3.** A comparison of energy evolution using different SAV schemes for the Cahn–Hilliard equation with various time steps. This figure illustrates the HSAV schemes can predict accurate solution with much larger time steps than the SAV-CN scheme.

Next, we study the power-law coarsening dynamics. Here we set  $\lambda=0.02$ ,  $\varepsilon=0.05$ , and domain  $\Omega=[0,4\pi]^2$ , and use the initial profile  $\phi(x,y,0)=0.001$ rand(x,y). It is known that the effective free energy decreases asymptotically following a power law  $E(t)\approx O(t^{-1/3})$ . We use the 4th, 6th order HSAV schemes and the SAV-CN scheme to calculate it, with  $256^2$  meshes and

 $\gamma_0=1$ ,  $C_0=1$ . The obtained results are summarized in Fig. 5. We observe that all the numerical schemes can capture the power law dynamics very well when the time step is small enough, saying when  $\Delta t=10^{-3}$ . However, the maximum time step of capturing the correct dynamics using the HSAV scheme is much larger than that of the SAV-CN scheme.

**Example 3** (*Molecular Beam Epitaxy Model*). In the last example, we consider the molecular beam epitaxy (MBE) growth model without slop selection [8]. Given the height profile of MBE denoted as  $\phi$ , the evolution equation is given by

$$\partial_t \phi = -M \Big( \varepsilon^2 \Delta^2 \phi + \nabla \cdot ((1 - |\nabla \phi|^2) \nabla \phi) \Big), \tag{49}$$

with periodic boundary conditions. The free energy in the model is given by

$$F = \int_{\Omega} \left( \frac{\varepsilon^2}{2} (\Delta \phi)^2 + \frac{1}{4} (|\nabla \phi|^2 - 1)^2 \right) d\mathbf{x},\tag{50}$$

with a constant mobility M.

If we denote  $\mathcal{G}=-M$ ,  $\mathcal{L}=\varepsilon^2\Delta^2-\gamma_0\Delta$  and  $g(\nabla\phi)=\frac{1}{4}(|\nabla\phi|^2-1-\gamma_0)^2+\frac{C_0}{|\Omega|}$ , and introduce the scalar auxiliary variable

$$q = \sqrt{(g, 1)},\tag{51}$$

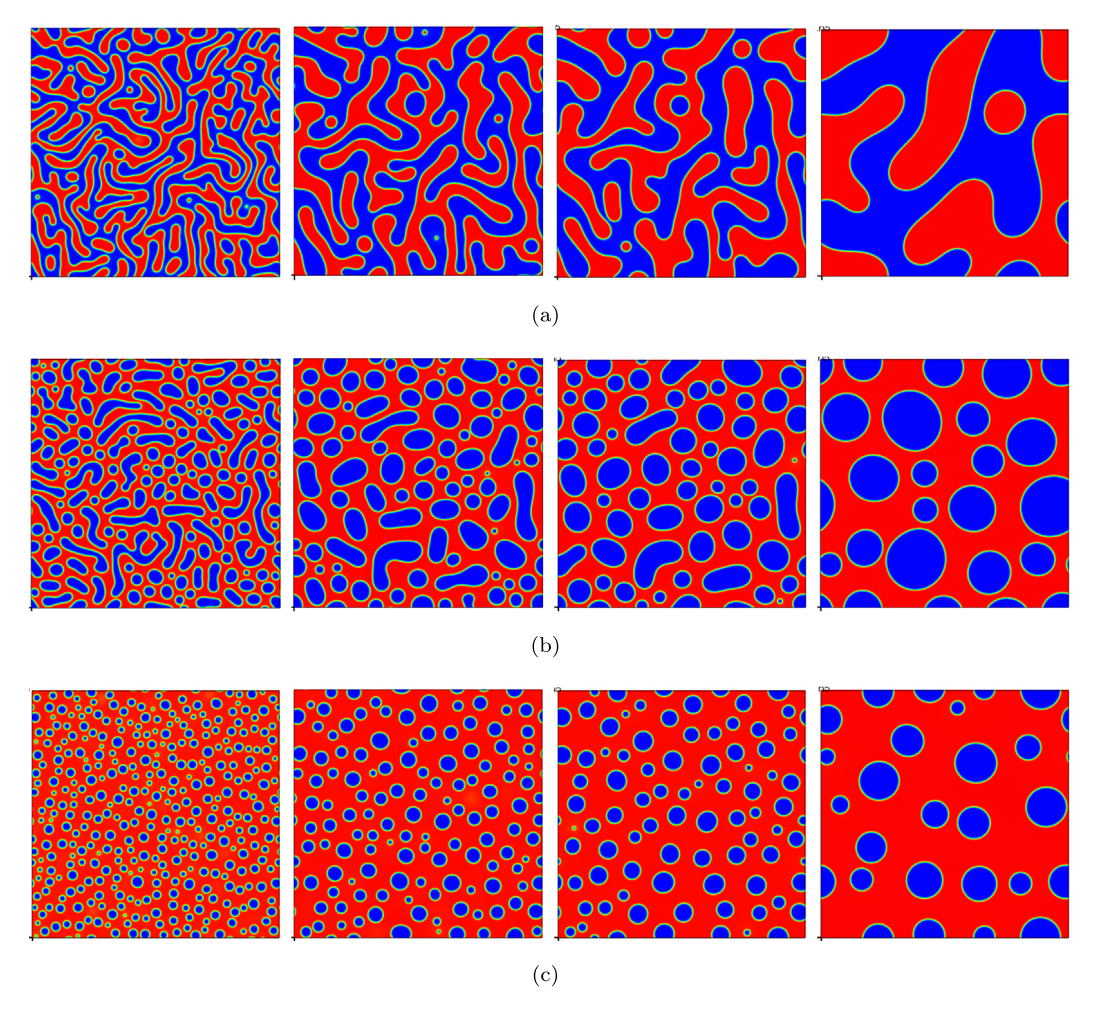


**Fig. 4.** Coarsening dynamics of a binary immersible fluid modeled by the Cahn–Hilliard equation using the 6th order HSAV scheme with time step  $\Delta t = 0.1$ . Here, we choose  $\phi_0 = 0, 0.1, 0.5$ , and the results at a few selected time slots are shown in (a)–(c) respectively. This figure presents the profile of  $\phi$  at time t = 10, 50, 100, 1000. It illustrates the HSAV scheme captures the phase separation dynamics accurately with fairly large time steps.

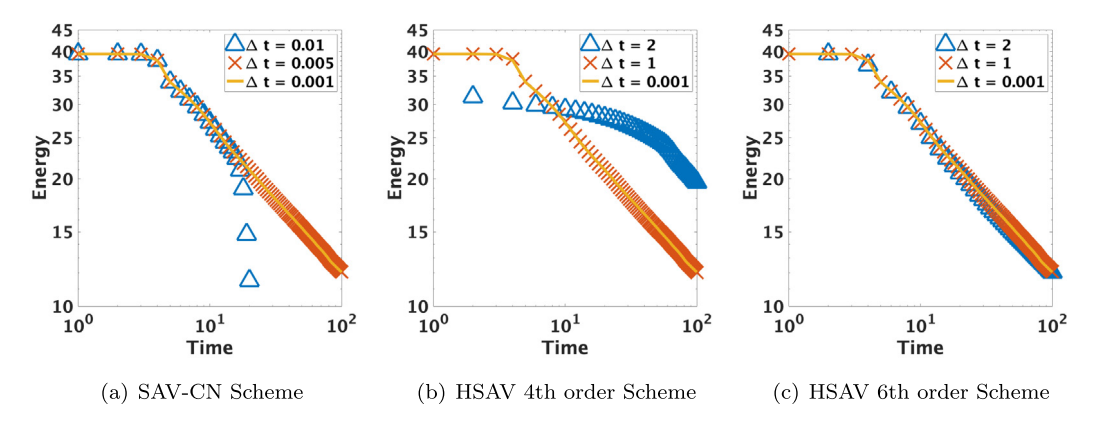


**Fig. 5.** Energy evolution of the Cahn–Hilliard equation in phase separation dynamics with different time steps. Here the log–log scale of the energy with respect to time is plotted. It illustrates that the higher order scheme performs better than lower order schemes in the simulations with large time steps.

and the intermediate function

$$H = \frac{\nabla \cdot \left( (\gamma_0 + 1 - |\nabla \phi|^2) \nabla \phi \right)}{2\sqrt{\int_{\Omega} \frac{1}{4} (|\nabla \phi|^2 - 1 - \gamma_0)^2 d\mathbf{x} + C_0}},$$
(52)

the equation can be reformulated as

$$\partial_t \phi = -M \Big( \varepsilon^2 \Delta^2 \phi - \gamma_0 \Delta \phi + 2qH \Big),$$

$$\frac{d}{dt} q = \Big( H, \partial_t \phi \Big),$$
(53)

with the consistent initial condition for q, i.e.  $q(t = 0) = \sqrt{(g, 1)}|_{t=0}$ .

First of all, we would like to test the convergence rate for our proposed schemes. Following the strategy in Example 1, we use Cauchy sequences, where the errors are calculated as the differences between numerical solutions with adjacent time steps. We set M=1,  $\varepsilon=1$  and the domain  $\Omega=[0,2\pi]^2$ . We use a smooth initial condition  $\phi(x,y,0)=\sin(x)\sin(y)$ , and choose  $\gamma_0=1$ ,  $C_0=1$ ,  $256^2$  meshes. The refinement-test results are summarized in Fig. 6. We observe that all the schemes reach their expected orders of convergence when the time-step is small enough. However, the HSAV schemes have dramatically smaller numerical errors (with several magnitudes smaller) than the SAV-CN scheme, which highlights the advantage of the newly proposed HSAV schemes.

Then, the proposed 4th-order and 6th-order HSAV schemes are tested via a benchmark problem [45]. Consider the domain  $\Omega = [0, 2\pi]^2$ , and parameters  $\varepsilon^2 = 0.1$ , M = 1. We pick the initial profile

$$\phi(x, y, 0) = 0.1(\sin(3x)\sin(2y) + \sin(5x)\sin(5y)).$$

This is a classic example that has been studied intensively [8,9]. The effective free energy dynamics using different schemes with various time steps are plotted in Fig. 7. We notice that even though all schemes assure the energy dissipation properties, the SAV-CN scheme requires a much smaller time step size (around  $\Delta t = 10^{-4}$ ) to predict accurate energy dissipation. In the meanwhile, the HSAV scheme can predict energy evolution accurately even with time step  $\Delta t = 0.05$ , which is 500 larger than the SAV scheme.

Besides, the total CPU time using each scheme to calculate the MBE model till t=15 is summarized in Table 3, where we observe the HSAV scheme is much faster than the low order SAV scheme, as much larger time steps can be used for HSAV scheme while preserving the desired accuracy.

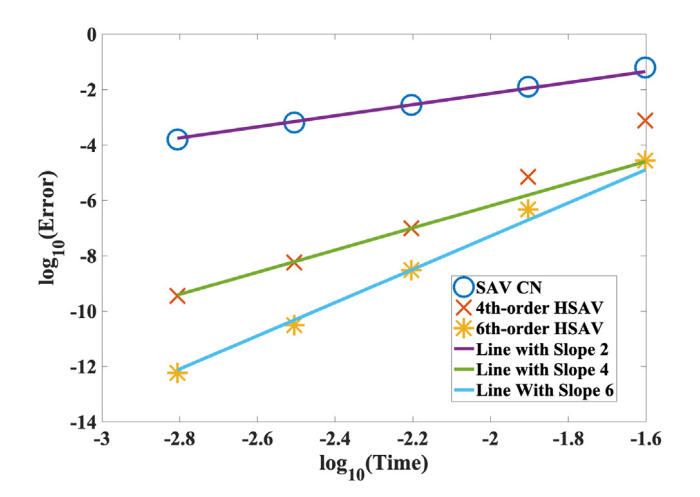


**Fig. 6.** Time step refinement test for the SAV schemes for the Molecular Beam Epitaxy model. This figure demonstrates the HSAV schemes reach their expected order of accuracy. The numerical error of the higher order schemes is dramatically smaller than the lower order schemes.

**Table 3**Total CPU time using various numerical schemes solving the MBE model.

	SAV-CN scheme	HSAV 4th-order scheme	HSAV 6th-order scheme
$\Delta t$	0.0001	0.025	0.05
CPU time (seconds)	672.39	79.45	74.72

One simulation using fourth order HSAV scheme with time step  $\Delta t=0.025$  is shown in Fig. 8, where the height profile of  $\phi$  at different times is shown. The patterns agree very well with the solution computed using other numerical solvers in the literature, while we can use an extremely larger time step than the time-step used in the other methods.

#### 6. Conclusion

In this paper, we combine the SAV approach with the structure-preserving discretization strategy to propose a new class of unconditionally energy stable methods for gradient flow models, which we name them the HSAV schemes. The HSAV scheme can reach arbitrarily high-order accuracy in time while respecting the discrete energy dissipation law in terms of the reformulated energy dissipation rate. Therefore, the schemes are more accurate than the available second order schemes and suitable for longtime dynamic simulations with larger time steps.

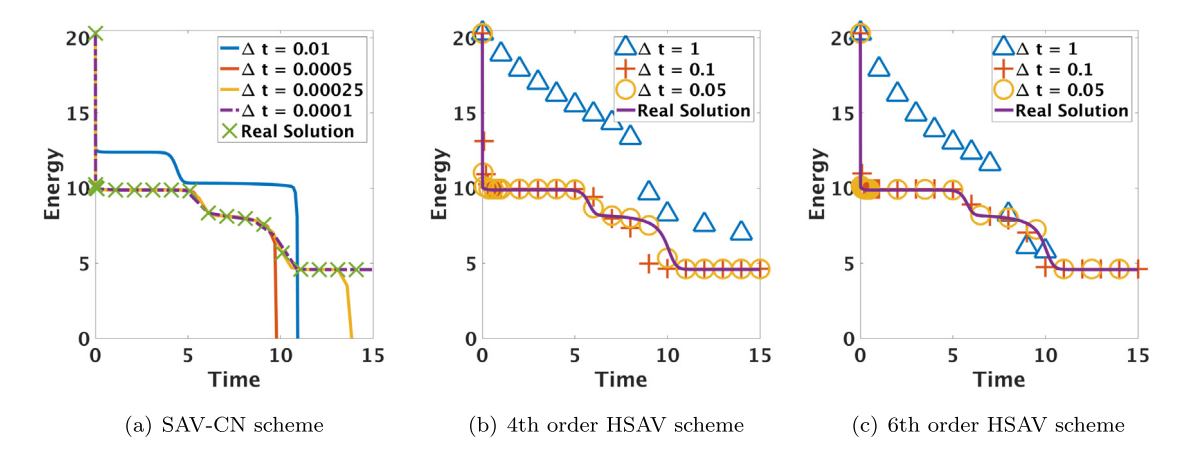
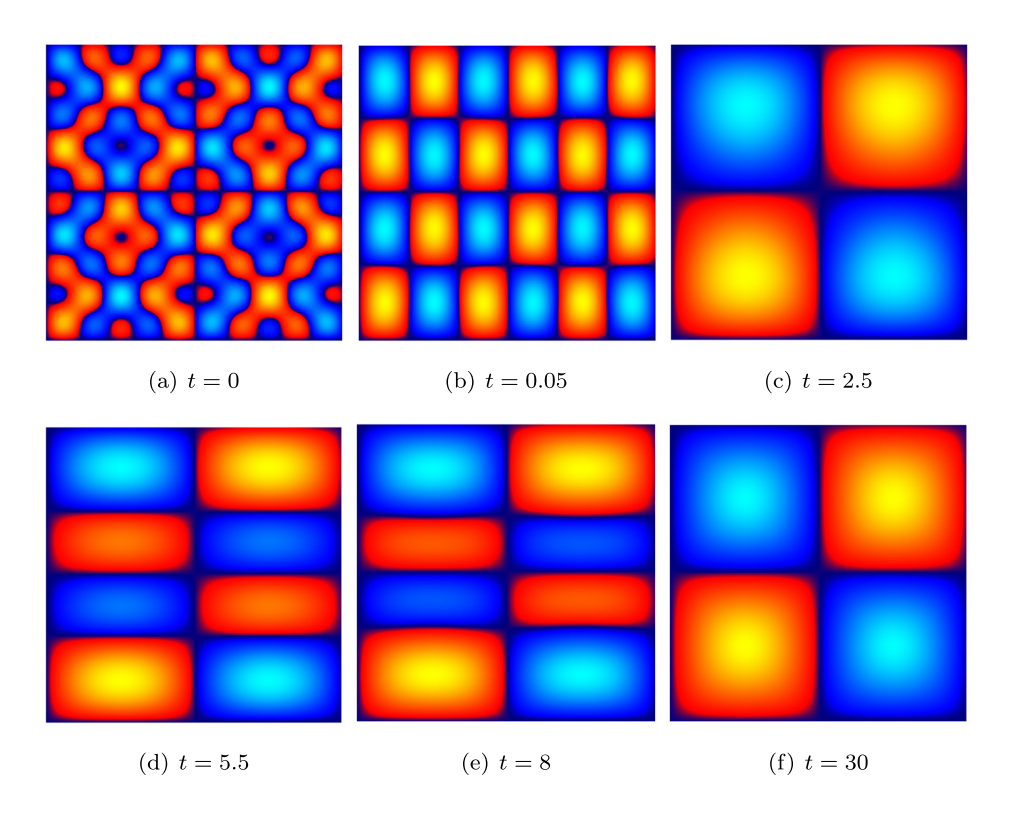


Fig. 7. Energy evolution in crystal growth modeled by MBE model and calculated by different SAV schemes with various time steps. This figure demonstrates the HSAV schemes can predict accurate energy dissipation dynamics with much larger time steps than the low order SAV scheme while solving the dynamical details in the MBE model with slope selection.



**Fig. 8.** The isolines of numerical solutions of the height function  $\phi$  for the MBE model with slope selection using the 4th order HSAV scheme. The time step is  $\Delta t = 0.025$ . Snapshots are taken at t = 0, 0.05, 2.5, 5.5, 8, 30, respectively.

Because of the enhanced accuracy, the HSAV schemes can dramatically improve transient dynamical simulations, giving the schemes based on energy quadratization methodology a competitive edge over the other methods in terms of simplicity, ease-of-implementation, energy-dissipation-rate preserving, and most importantly high order of accuracy. Some numerical benchmarks are presented to illustrate the outstanding performance of the proposed numerical methods. The proposed HSAV method is rather general, applicable to any gradient flow models derived through energy variation. Furthermore, it can also be generalized to study thermodynamically-consistent hydrodynamic models, where additional conservation laws appear as constraints.

#### **Declaration of competing interest**

The authors declare that they have no known competing financial interests or personal relationships that could have appeared to influence the work reported in this paper.

#### Acknowledgments

Yuezheng Gong's work is partially supported by the Natural Science Foundation of Jiangsu Province, China (Grant No. BK20180413) and the National Natural Science Foundation of China (Grant No. 11801269). Jia Zhao's work is partially supported by National Science Foundation, USA under Grant Number NSF

DMS-1816783. Qi Wang's research is partially supported by NSF, USA awards DMS-1517347, DMS-1815921, OIA-1655740 and a GEAR, USA award from SC EPSCoR/IDeA Program.

#### References

- [1] L. Onsager, Phys. Rev. 37 (1931) 405-426.
- [2] L. Onsager, Phys. Rev. 38 (1931) 2265-2279.
- [3] J. Zhao, X. Yang, Y. Gong, X. Zhao, X. Yang, J. Li, Q. Wang, Int. J. Numer. Anal. Model. 15 (6) (2018) 884–918.
- [4] X. Yang, J. Li, G. Forest, Q. Wang, Entropy 18 (6) (2016) 202.
- [5] J. Shen, J. Xu, J. Yang, J. Comput. Phys. 353 (2018) 407-416.
- [6] S.M. Allen, J.W. Cahn, Acta Metall. 20 (423) (1972).
- [7] J.W. Cahn, J.E. Hilliard, J. Chem. Phys. 28 (1958) 258–267.
- [8] C. Wang, X. Wang, S. Wise, Discrete Contin. Dyn. Syst. 28 (1) (2010) 405–423.
- [9] L. Chen, J. Zhao, X. Yang, Appl. Numer. Math. 128 (2018) 138-156.
- [10] B. Gonzalez-Ferreiro, H. Gomez, I. Romero, Commun. Nonlinear Sci. Numer. Simul. 19 (2014) 2309–2323.
- [11] S. Wang, R. Sekerka, A. Wheeler, B.T. Murray, S.R. Coriell, R.J. Braun, G.B. McFadden, Physica D 69 (1993) 189–200.
- [12] F. Boyer, C. Lapuerta, ESAIM Math. Model. Numer. Anal. 40 (2006) 653-687.
- [13] J. Kim, Commun. Comput. Phys. 12 (3) (2012) 613–661.
- [14] D.J. Eyre, Mrs Online Proc. Libr. Arch. 529 (1998) 39–46.
- [15] C. Wang, S. Wise, SIAM J. Numer. Anal. 49 (3) (2011) 945-969.
- [16] J. Shen, X. Yang, Discrete Contin. Dyn. Syst. A 28 (2010) 1669-1691.
- [17] I. Romero, Internat. J. Numer. Methods Engrg. 79 (2009) 706–732.
- [18] F. Guillen-Gonzailez, G. Tierra, J. Comput. Phys. 234 (2013) 140-171.
- [19] V.E. Badalassi, H.D. Ceniceros, S. Banerjee, J. Comput. Phys. 190 (2) (2003) 371–397
- [20] Y. Li, J. Kim, N. Wang, Commun. Nonlinear Sci. Numer. Simul. 53 (2017) 213–227.
- [21] W. Hu, M. lai, East Asian J. Appl. Math. 3 (3) (2013) 247-262.

- [22] L. Ju, X. Li, Z. Qiao, H. Zhang, Math. Comp. 87 (312) (2018) 1859-1885.
- [23] W. Chen, S. Conde, C. Wang, X. Wang, S. Wise, J. Sci. Comput. 52 (2012) 546–562.
- [24] Z. Guo, P. Lin, J. Lowengrub, S. Wise, Comput. Methods Appl. Mech. Engrg. 326 (2017) 144–174.
- [25] X. Yang, J. Zhao, X. He, J. Comput. Appl. Math. 343 (2018) 80-97.
- [26] X. Yang, J. Zhao, Commun. Comput. Phys. 25 (2019) 703-728.
- [27] S. Badia, F. Guillen-Gonzalez, J. Gutierrez-Santacreu, J. Comput. Phys. 230 (2011) 1686–1706.
- [28] F. Guillen-Gonzalez, G. Tierra, Comput. Math. Appl. 68 (8) (2014) 821–846.
- [29] X. Yang, J. Zhao, Q. Wang, J. Shen, Math. Models Methods Appl. Sci. 27 (2017) 1993–2023.
- [30] Y. Gong, J. Zhao, Q. Wang, SIAM J. Sci. Comput. 40 (2) (2018) B528-B553
- [31] Y. Gong, J. Zhao, X. Yang, Q. Wang, SIAM J. Sci. Comput. 4 (1) (2018) B138–B167.
- [32] D. Han, A. Brylev, X. Yang, Z. Tan, J. Sci. Comput. 70 (3) (2017) 965-989.
- [33] J. Shen, J. Xu, J. Yang, SIAM Review 61 (3) (2019) 474-506.
- [34] R. Guo, Y. Xu, Commun. Comput. Phys. 26 (1) (2019) 87–113.
- [35] J. Shin, H. Lee, J. Lee, J. Comput. Phys. 347 (2017) 367–381.
- [36] Y. Gong, J. Zhao, Appl. Math. Lett. 94 (2019) 224-231.
- [37] Y. Gong, J. Zhao, Q. Wang, Arbitrarily high-order unconditionally energy stable schemes for thermodynamically consistent gradient flow models, 2019, arXiv:1907.05341.
- [38] E. Hairer, C. Lubich, G. Wanner, Geometric Numerical Integration: Structure-Preserving Algorithms for Ordinary Differential Equations, vol. 31. Springer, 2006.
- [39] J. Chen, M. Qin, Electron. Trans. Numer. Anal. 12 (2001) 193-204.
- [40] Y. Gong, J. Zhao, Q. Wang, Adv. Comput. Math. 44 (2018) 1573-1600.
- [41] Y. Gong, J. Cai, Y. Wang, Commun. Comput. Phys. 16 (1) (2014) 35-55.
- [42] T. Tang, J. Yang, J. Comput. Math. 34 (5) (2016) 471-481.
- [43] L.Q. Chen, Annu. Rev. Mater. Res. 32 (1) (2002) 113–140.
- [44] H. Gomez, T.J.R. Hughes, J. Comput. Phys. 230 (13) (2011) 5310–5327.
- [45] X. Yang, J. Zhao, Q. Wang, J. Comput. Phys. 333 (2017) 102-127.